Donor strand sequence, rather than donor strand orientation, determines the stability and non-equilibrium folding of the type 1 pilus subunit FimA

Received for publication, May 11, 2020, and in revised form, July 7, 2020 Published, Papers in Press, July 10, 2020, DOI 10.1074/jbc.RA120.014324

Dawid Zyla[‡], **Blanca Echeverria**[‡], **and Rudi Glockshuber***

From the Institute of Molecular Biology and Biophysics, ETH Zurich, Zurich, Switzerland

Edited by Wolfgang Peti

FimA is the main structural subunit of adhesive type 1 pili from uropathogenic *Escherichia coli* strains. Up to 3000 copies of FimA assemble to the helical pilus rod through a mechanism termed donor strand complementation, in which the incomplete immunoglobulin-like fold of each FimA subunit is complemented by the N-terminal extension (Nte) of the next subunit. The Nte of FimA, which exhibits a pseudo-palindromic sequence, is inserted in an antiparallel orientation relative to the last β-strand of the preceding subunit in the pilus. The resulting subunit-subunit interactions are extraordinarily stable against dissociation and unfolding. Alternatively, FimA can fold to a self-complemented monomer with anti-apoptotic activity, in which the Nte inserts intramolecularly into the FimA core in the opposite, parallel orientation. The FimA monomers, however, show dramatically lower thermodynamic stability compared with FimA subunits in the assembled pilus. Using self-complemented FimA variants with reversed, pseudo-palindromic extensions, we demonstrate that the high stability of FimA polymers is primarily caused by the specific interactions between the side chains of the Nte residues and the FimA core and not by the antiparallel orientation of the donor strand alone. In addition, we demonstrate that nonequilibrium two-state folding, a hallmark of FimA with the Nte inserted in the pilus rod-like, antiparallel orientation, only depends on the identity of the inserted Nte side chains and not on Nte orientation.

Type 1 pili of uropathogenic *Escherichia coli* (UPEC) strains are filamentous surface protein complexes that mediate pathogen attachment to urinary epithelium cells by binding high-mannose-type glycans of surface glycoproteins via the lectin FimH at their distal tip (1–4). The type 1 pilus is composed of the helical pilus rod formed by up to 3000 copies of the main pilus subunit FimA and a linear tip fibrillum formed by the minor subunits FimF and FimG and the adhesin FimH. Pilus assembly *in vivo* proceeds via the chaperone-usher pathway (5), in which the periplasmic chaperone FimC catalyzes the folding of the pilus subunits as soon as their invariant, structural disulfide bond is formed by disulfide exchange with the periplasmic dithiol oxidase DsbA (6). FimC then delivers the folded subunits to the assembly platform (usher) FimD in the outer membrane (7), where FimD catalyzes subunit assembly and mediates subunit translocation across the outer membrane (Fig. 1*A*) (8, 9).

The subunits in the assembled pilus form highly stable interactions that confer infinite stability against spontaneous dissociation to the pilus (10, 11). The common mechanism of the subunit-subunit interactions is termed donor strand complementation, in which the incomplete, immunoglobulin-like (pilin) fold of each subunit, lacking the C-terminal β-strand, is completed by insertion of the N-terminal ~20-residue extension of the following subunit that provides the missing β-strand (12, 13). Specifically, the N-terminal extension (Nte, also termed donor strand) of the next subunit inserts in an antiparallel orientation relative to the C-terminal β-strand F of the pilin fold into a long hydrophobic groove in the pilin domain. The groove contains 5 pockets (P1–P5), which specifically accommodate hydrophobic Nte side chains (12, 14, 15).

The main pilus subunit FimA from type 1 piliated, enteroinvasive pathogens (*E. coli* FimA: 159 residues, 15.8 kDa) differs from all other pilus subunits in that it possesses two alternative folding possibilities: (i) it can assemble to the helical, homopolymeric pilus rod (16) via the canonical, antiparallel donor strand complementation mechanism or (ii) can fold to soluble, self-complemented monomers in which the Nte inserts intramolecularly into the FimA fold in the opposite, parallel orientation (10, 17). These alternative folding possibilities become possible due to a pseudo-palindromic sequence in the Nte of FimA (. . .Gly^{8}-*Z*-*X*-His^{11}-*X*-*Z*-Gly^{14}. . . in *E. coli* FimA), with His^{11} in the center of the palindrome, where *X* is a hydrophobic residue and *Z* is a hydrophilic/charged residue (. . .Gly^{8}-Thr^{9}-Val^{10}-His^{11}-Phe^{12}-Lys^{13}-Gly^{14}. . .). The solved three-dimensional structures of both *E. coli* FimA conformers showed that the residues Gly^{8} and Gly^{14}, which occupy the shallow P4 pocket in the FimA monomer and the FimA polymer, respectively, define the register of the inserted Nte β-strand. The P4 pocket is so shallow that it can only accommodate a glycine residue without disturbing the main-chain β-sheet hydrogen-bonding network between the inserted Nte and the neighboring strands A and F of the FimA fold (Fig. 1*B*) (10, 14, 17). The vast majority of the FimA molecules secreted into the *E. coli* periplasm bind to the assembly chaperone FimC, fold when bound to FimC, and are delivered as FimA-FimC complexes to the assembly platform FimD. However, a small fraction of the FimA molecules appears to fold independently of FimC to soluble monomers. These FimA monomers act as inhibitors of apoptosis of urinary epithelium cells after type 1 pilus-mediated UPEC

This article contains supporting information.
[‡] These authors contributed equally to this work.
* For correspondence: Rudi Glockshuber, rudi@mol.biol.ethz.ch.

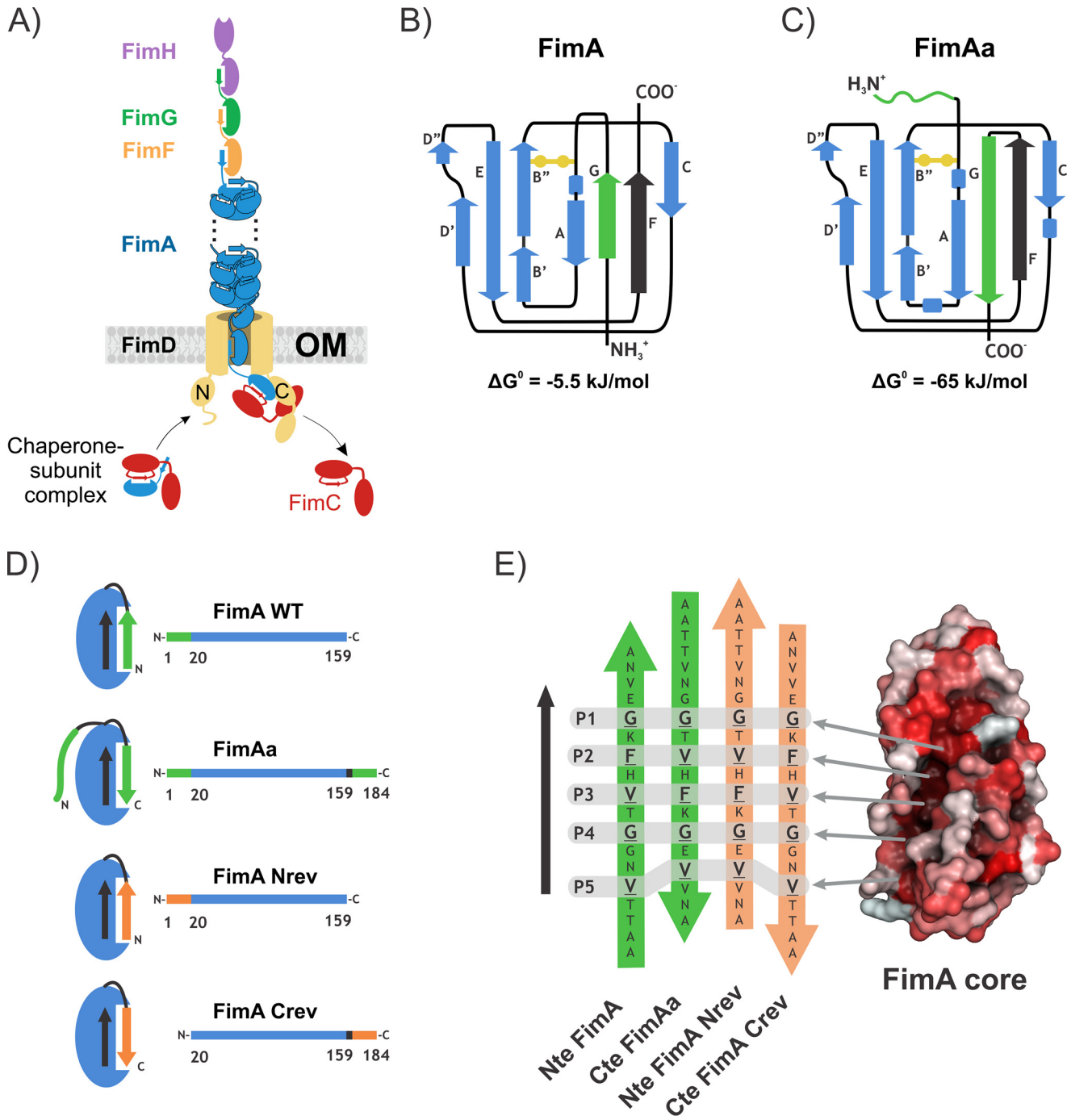

Figure 1. Alternative folding possibilities of the main type 1 pilus subunit FimA and FimA constructs used in this study. *A*, composition and assembly of type 1 pili via the chaperone-usher pathway. The helical pilus rod is composed of up to 3000 copies of FimA and anchored to FimD in the outer membrane (*OM*), which catalyzes pilus assembly from FimC-subunit complexes in the periplasm. The subunits FimF, FimG, and the adhesin FimH form the distal tip fibrillum. *B*, β-sheet topology diagram of the marginally stable FimA monomer, with intramolecular, parallel Nte insertion into the FimA fold. *C*, β-sheet topology diagram of FimAa, in which a second FimA donor strand copy is fused to the FimA C terminus. FimAa molecules exclusively adopt the more stable conformer in which the C-terminal donor strand (Cte) is inserted in the "antiparallel" orientation into the FimA fold. *D*, schematic representation of the FimA constructs used in this study. WT donor strands are *colored* in *green*, and donor strands with a reversed amino acid sequence are depicted in *orange*. The $(Gly)_6$ linker between the FimA C terminus and the Cte is shown in *black*. The last β-strand (F strand) of FimA WT is shown in *black* as a reference. *E*, primary structures of the donor strands in the FimA variants shown in *D* in the context of the respective tertiary structure. The FimA core (residues 20–159) is shown as a *surface representation* with normalized Eisenberg hydrophobicity scale (29) (*white*, hydrophilic; *red*, hydrophobic). As in *D*, the *black arrow* indicates the reference F strand. The five binding pockets P1–P5 specifically accommodating residues of the inserted donor strand are indicated on a *gray background*. The shallow pockets P1 and P4 can only accommodate glycines, whereas P2 and P3 can accommodate either valine or phenylalanine side chains.

internalization. This mechanism may enable UPEC strains to escape antibiotic treatment during urinary tract infections inside the host cells (18).

The two alternative modes of Nte insertion into the FimA fold have dramatic consequences for folding and thermodynamic stability of FimA. Guanidinium chloride (GdmCl)-

induced unfolding/refolding equilibria showed that the self-complemented *E. coli* FimA monomer exhibits only marginal thermodynamic stability. Unfolding/refolding equilibria of the *E. coli* FimA monomer were attained after 1 day of incubation and revealed free energy of folding of only −5.5 kJ/mol at pH 7.0 and 25 °C (10, 14). In contrast, a self-complemented FimA variant (FimAa), mimicking the state of FimA in the assembled pilus rod, proved to be extremely stable, with a free energy of folding of −66.5 kJ/mol (10, 14). In FimAa, a second copy of the 19-residue Nte sequence was fused to the FimA C terminus via a hexaglycine linker. This C-terminal Nte inserts in the antiparallel orientation into the FimA fold, whereas the natural Nte at the N terminus stays flexibly disordered (Fig. 1, *C* and *D*). In addition, FimAa showed very high activation energy barriers for unfolding and refolding so that the folding equilibrium could never be attained at 25 °C. Specifically, the unfolding of FimAa after incubation for 1 day could only be observed at GdmCl concentrations above 5 M, whereas refolding could only be detected below 1 M GdmCl. Nevertheless, global fits of the unfolding and refolding transitions of FimAa, recorded after different incubation times (1–30 days), proved to be fully consistent with the two-state model of folding. These results showed that the extraordinary stability of FimA in the context of the assembled pilus is based on its essentially infinite stability against unfolding/dissociation under physiological conditions, as the extrapolated $t_{1/2}$ of spontaneous FimAa unfolding at pH 7.0, 25 °C, and zero GdmCl proved to be in the range of 100 million years (10).

In the present study, we addressed the question of whether the extraordinary stability of FimA with the Nte inserted in the antiparallel orientation (intramolecular in FimAa, intermolecular in FimA/FimA contacts in the pilus rod) primarily originates from antiparallel β-strand insertion or from specific interactions between the Nte side chains of the Nte pseudo-palindrome in the binding pockets P1–P5. For this purpose, we compared the stability of FimA and FimAa with that of two analogous FimA variants, FimA Nrev and FimA Crev, in which the entire Nte sequence was reversed (Fig. 1, *D* and *E* and Fig. S1). In FimA Nrev, the sequence of the first 19 FimA residues was reversed relative to WT FimA. In the variant FimA Crev, the reversed Nte sequence was fused to the C terminus via a hexaglycine linker, and the natural Nte was deleted. We demonstrate that the two characteristic features of FimA in the context of the pilus rod, extraordinary stability against unfolding and unattainable folding equilibria under physiological conditions, are mainly governed by the identity of the Nte side chains inserting in the P1–P5 pockets of the FimA fold.

Results

Production and purification of FimA Nrev and FimA Crev

All FimA variants were produced in the *E. coli* cytoplasm under the control of the T7 promoter without the natural FimA signal sequence. Due to the reducing conditions in the cytoplasm, all variants were unable to form the conserved structural disulfide bond and accumulated as insoluble inclusion bodies. As described previously for FimA and FimAa, precipitated FimA Nrev and FimA Crev were solubilized by 6 M GdmCl (10). After the formation of the structural disulfide bond by Cu^{2+}-catalyzed air oxidation in the presence of denaturant, the variants were refolded by removal of the denaturant through dialysis. Refolded proteins were concentrated and purified by gel filtration on Superdex 75 columns, in which they eluted at the retention volume corresponding to the folded FimA monomer. The average yield of purified FimA variants was about 35 mg/liter of bacterial culture. MS confirmed that the N-terminal methionine had been cleaved in all FimA variants.

Stability of the FimA variants against thermal unfolding

In a first experiment to probe the stability of FimA WT relative to that of FimA Nrev and of FimAa relative to that of FimA Crev, we recorded thermal unfolding transitions of all proteins at pH 7.0 via the loss of the native far-UV CD signal at 230 nm. Reversal of the Nte in FimA monomers (parallel orientation) caused a strong stabilization in the FimA Nrev variant, with an increase in the apparent melting temperature (T_m) by 17 °C, from 49 (FimA WT) to 66 °C (FimA Nrev) (Fig. 2). An analogous result was obtained for the reversal of the donor strand sequence attached to the C terminus of FimA (antiparallel orientation): whereas FimAa showed extraordinary stability with an apparent T_m of 95 °C, the T_m of the protein dropped to 49 °C in the variant FimA Crev (*i.e.* the T_m observed for the FimA WT monomer) (Fig. 2). Together, the thermal unfolding data indicated that the Nte residues inserting into the P1–P5 pockets of the pilin fold of FimA are critical determinants for the stability of donor strand–complemented FimA and that the antiparallel donor strand orientation alone is not sufficient to explain the extraordinary stability of FimA subunits in the assembled pilus.

Donor strand side chains interacting with the P1–P5 pockets of the FimA fold determine thermodynamic stability and the dynamics of the two-state folding equilibrium of donor strand–complemented FimA

Next, we measured GdmCl-dependent unfolding and refolding transitions at pH 7.0 and 25 °C of FimA Nrev and FimA Crev. Fig. 3*A* shows that FimA Crev, similar to the FimA WT monomer, attained its folding equilibrium after incubation for 1 day. Like FimA, FimA Crev proved to be only marginally stable, with a free energy of folding (ΔG^0) of −6.9 ± 1.8 kJ/mol. This value is identical within experimental error to the previously reported stability of FimA WT monomers (−5.5 ± 0.5 kJ/mol) under exactly the same conditions (Tables 1 and 2). This result is consistent with the virtually identical stabilities against thermal unfolding of FimA WT and FimA Crev (Fig. 2).

As observed previously for FimAa, the unfolding/refolding transitions (recorded after 1 and 8 days of incubation) of FimA Nrev differed drastically from those observed for FimA and FimA Crev. Specifically, even after incubation for 8 days, the folding equilibrium of FimA Nrev could not be attained, because unfolding could only be observed at high and refolding only at low denaturant concentrations (Fig. 3*B*). The global analysis of all unfolding and refolding transitions proved to be fully consistent with a kinetically unattained two-state equilibrium with a very high activation energy barrier for unfolding

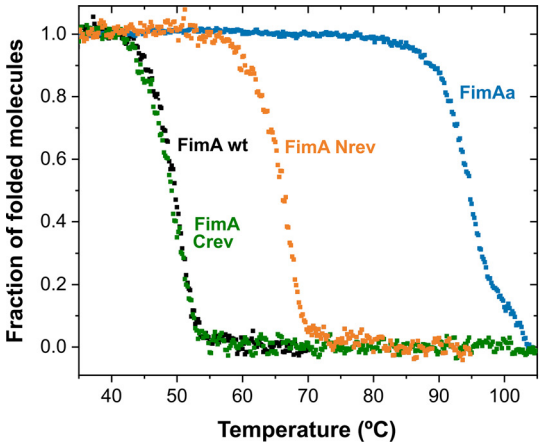

Protein variant	Apparent melting temperature (°C)
FimA WT	49
FimA Crev	49
FimA Nrev	66
FimAa	95

Figure 2. Temperature-induced unfolding transitions of FimA WT, FimAa, FimA Crev, and FimA Nrev at pH 7.0. The unfolding of FimA WT (*black*), FimAa (*blue*), FimA Crev (*green*), and FimA Nrev (*orange*) was measured by following the CD signal decrease at 230 nm with increasing temperature. The transitions were consistent with a single unfolding transition. The CD traces were tentatively evaluated according to the van't Hoff equation and normalized. The obtained apparent melting temperatures of all variants are listed in the *right panel*.

and refolding. Fig. 3*C* shows the logarithm of the observed rate constant (k_{obs}) of equilibrium attainment ($k_{obs} = k_F + k_U$) dependence on the denaturant concentration deduced from the nonequilibrium data in Fig. 3*B*, which allowed calculating the free energy of folding (ΔG^0) and the rate constants of folding and unfolding at zero denaturant of FimA Nrev (Tables 1 and 2). The obtained ΔG^0 value of -31.5 ± 1.3 kJ/mol shows that FimA Nrev is 26 kJ/mol (~5 times) more stable than the FimA WT monomer. As FimA WT and FimA Nrev show the same (parallel) donor strand orientation and only differ in their reversed Nte sequences, the results clearly demonstrate that essentially only the Nte residues interacting with the pockets P1–P5 of the FimA pilin fold determine the characteristic features of FimA subunits in the assembled pilus rod: extraordinary thermodynamic stability and extreme kinetic stability against unfolding and dissociation (Tables 1 and 2).

All FimA variants fold very slowly and with similar rates

We previously showed that the *E. coli* FimA WT monomer and FimAa variant spontaneously refold very slowly and with very similar half-lives of about 2 h (10, 14), indicating that residues that form the Nte do not contribute to the stability of the transition state of folding. This predicted that the FimA variants FimA Nrev and FimA Crev also fold slowly with similar rates. To test this hypothesis, we recorded the refolding kinetics at pH 7.0 and 25 °C of FimA Nrev, FimA Crev, FimA, and FimAa under the same conditions (50 mM final GdmCl concentration after rapid dilution with refolding buffer). Indeed, all FimA variants refolded with essentially the same kinetics (half-lives between 1.6 and 2.6 h), indicating that the transition states of folding are very similar for the four FimA variants (Fig. 4). For the FimAa and FimA Nrev variants, which did not attain folding equilibrium at 25 °C (Tables 1 and 2), the measured half-lives of folding in 50 mM GdmCl (Fig. 4, *B* and *D*, respectively) agreed well (within a factor of 2) with those predicted from their nonequilibrium transitions for folding at the same GdmCl concentration (Fig. 3). The data are consistent with a model in which the transition state of FimA folding is only formed by the residues 20–159 of the FimA fold (see Fig. 1) (14). Segment 20–159 is the same in all FimA variants investigated. In addition, the fact that neither the orientation of the β-strand that complements the FimA fold nor its sequence influences the FimA folding kinetics explains why all variants fold with essentially the same kinetics although their thermodynamic stabilities are dramatically different.

Crystal structures of FimA Nrev and FimA Crev

To test whether the reversed sequences of the N- and C-terminal extensions in the FimA Nrev and FimA Crev constructs indeed inserted as predicted into the FimA fold, we solved the X-ray structures of both variants at 1.8 and 1.5 Å, respectively, by molecular replacement using the X-ray structure of FimA (PDB entry 5NKT) as a search model (Fig. 5 and Table 3). Superposition of the C^α carbon traces of FimA and FimA Nrev and of FimAa and FimA Crev showed that the sequence reversal of the N- and C-terminal extension, respectively, could be very well accommodated by the immunoglobulin-like FimA fold (C^α RMSD values of 0.24 and 0.98 Å, respectively; see Fig. S3 for the local per residue RMSD values in the donor strand regions). As predicted, the register of β-strand insertion of the reversed Nte/Cte segments remained unchanged and dictated by the glycine residues occupying the P1 and P4 pockets of the FimA fold (Fig. S3, *left panels*). In addition, the structures of all four FimA variants demonstrated that both the P2 and P3 pocket can accommodate either valine or phenylalanine side chain, independently of the orientation of the donor strand. Despite the dramatic differences in thermodynamic stability between FimA and FimA Nrev and between FimAa and FimA Crev (Tables 1 and 2), we could not find specific structural parameters that could directly explain these large stability differences (Table S2). The only peculiarity in the more stable structures FimAa and FimA Nrev was that their oppositely oriented donor strands aligned well over a wider range of residues compared with the oppositely oriented donor strands in the less stable variants FimA and FimA Crev (Fig. S3*F*). Specifically, the C^α RMSD values remained below 3 Å within a contiguous 12-residue segment of the donor strand (positions 2–13 of WT FimA) in the FimAa/FimA Nrev pair (Fig. S3*F*), whereas only

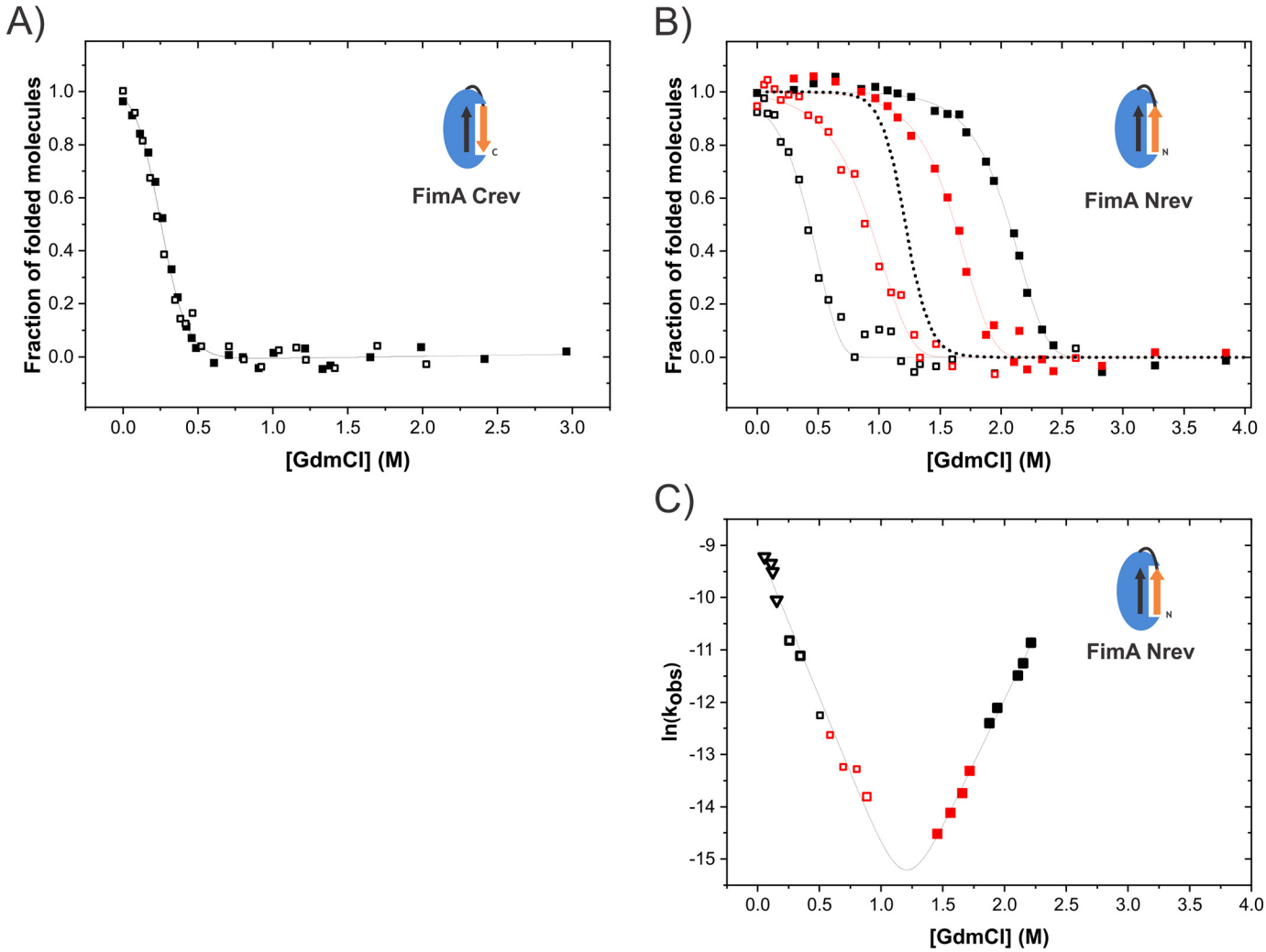

Figure 3. GdmCl-dependent unfolding and refolding transitions of FimA Nrev and FimA Crev at 25 °C and pH 7.0. *A*, unfolding (*filled black squares*) and refolding transitions (*open black squares*) of FimA Crev after 1 day of incubation at 25 °C. The coinciding unfolding and refolding transitions demonstrate that the folding equilibrium had been attained after 1 day (*solid line*; fit according to the two-state model of folding). The deduced thermodynamic stability parameters of FimA Nrev and FimA Crev are shown in Tables 1 and 2. *B*, normalized unfolding (*filled squares*) and refolding (*open squares*) transitions of FimA Nrev after incubation at 25 °C for 1 day (*black symbols*) and 8 days (*red symbols*). All unfolding and refolding traces of FimA Nrev were consistent with an unattained two-state equilibrium and fitted globally (*solid lines*). The *black*, *dotted line* indicates the transition after attainment of equilibrium, calculated from the parameters in Tables 1 and 2. *C*, plot of the observed rate constants of folding/unfolding ($k_{obs} = k_F + k_U$) of FimA Nrev, deduced from the data points in the transition regions in *B* from which first-order rate constants could be deduced (*same symbols* as in *B*). The *black triangles* correspond to the rate constants of refolding at low denaturant concentration recorded directly with far-UV CD kinetics.

Table 1

Thermodynamic and kinetic folding parameters of the FimA variants: Variants with donor strand side chains inserting into the FimA fold as observed in FimA WT monomers

Construct	ΔG^0	m_{eq}	$D_{½}$
	kJ mol^{-1}	*kJ mol*$^{-1}$ *M*$^{-1}$	*M*
FimA WT[a,b]	−5.50 ± 0.50	23.0 ± 1.3	0.24
FimA Crev[a]	−6.85 ± 1.77	27.9 ± 2.8	0.25

[a] Constructs that attain a folding equilibrium within 1 day.
[b] Data from Ref. 10.

seven contiguous donor stand residues (positions 8–14 of WT FimA) showed C^{α} RMSD values below 3 Å in the FimA/FimA Crev pair (Fig. S3*E*). Tables 1 and 2 and Fig. 4 demonstrate that all four FimA variants fold according to the two-state model and that differences in thermodynamic stability exclusively originate from huge differences in the rate constants of unfolding. The two-state folding predicts that all interactions stabilizing the native state are broken simultaneously upon unfolding. Thus, even small local structural changes could strongly influence the highly cooperative unfolding reaction when they have short- and long-range effects on neighboring native interactions.

Fig. 5*B* shows the structural comparison for the pairs of FimA variants with similar thermodynamic stability, in which the pockets P1–P5 are occupied by identical residues but the donor strands have the opposite orientation. Again, both pairs of structures proved to be highly similar (low stability: FimA/FimA Crev pair, C^{α} RMSD = 0.39 Å; high stability: FimAa/FimA Nrev pair: C^{α} RMSD = 0.97 Å; see Fig. S4 and Table S2 for all other pairwise comparisons). Despite their opposite orientation, the donor strands aligned almost perfectly within the pseudo-palindromic segments 5–14, and the conformations of the identical side chains in the pockets P1–P5 remained essentially the same (Fig. S3). Together, the structural data confirm

Table 2

Thermodynamic and kinetic folding parameters of the FimA variants: Variants with donor strand side chains inserting into the FimA fold as observed in FimA-FimA interactions in the assembled pilus rod

Construct	ΔG^0	m_{eq}	m_F	m_U	$D_{½}$	$k_F^{H_2O}$	$k_U^{H_2O}$	T_{eq} [a]
	$kJ\ mol^{-1}$	$kJ\ mol^{-1}\ M^{-1}$	M^{-1}	M^{-1}	M	s^{-1}	s^{-1}	
FimAa[b,c]	-66.5 ± 2.8	25.7 ± 0.9	-6.3 ± 0.3	4.1 ± 0.2	2.6 ± 0.1	$7.5 \pm 1.9 \cdot 10^{-5}$	$1.6 \pm 1.8 \cdot 10^{-16}$	3225 years
FimA Nrev[b]	-31.5 ± 1.3	26.4 ± 0.9	-5.7 ± 0.2	4.9 ± 0.3	1.2 ± 0.1	$1.2 \pm 0.1 \cdot 10^{-4}$	$3.6 \pm 1.9 \cdot 10^{-10}$	63 days

[a] Calculated time to reach equilibrium (<2% CD signal difference between unfolding and refolding).
[b] Constructs that did not attain a folding equilibrium within 8 days.
[c] Data from Ref. 10.

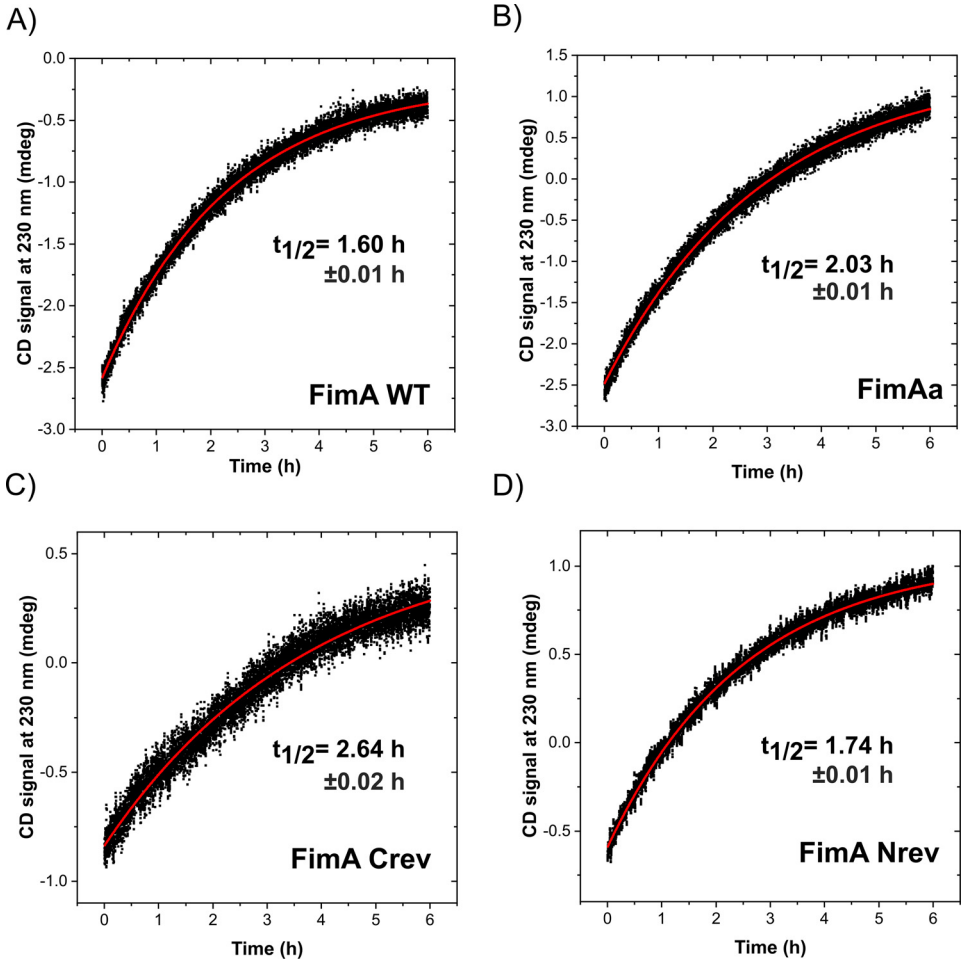

Figure 4. Refolding kinetics of FimA WT, FimAa, FimA Crev, and FimA Nrev at pH 7.0, 25 °C, and a residual GdmCl concentration of 50 mM. Secondary structure formation during refolding of FimA WT (*A*), FimAa (*B*), FimA Crev (*C*), and FimA Nrev (*D*) was monitored via an increase in the far-UV CD signal at 230 nm. Refolding traces were fitted with a single exponential function (*continuous red lines*), and the deduced half-lives are indicated with S.E. from the fits.

that the identity of the side chains in the pockets P1–P5, and not the orientation of the donor strand that inserts into the FimA fold, is the main determinant of the stability and folding kinetics of FimA.

Stabilization of FimA monomers prevents spontaneous assembly to pilus rods

The assembly of FimA to homopolymers that form the helical quaternary structure of the pilus rod is catalyzed *in vivo* by the periplasmic folding catalyst FimC (6, 14) and the assembly platform FimD in the outer membrane (19). Purified FimA monomers can however also assemble spontaneously to pilus rods *in vitro* in the absence of catalysts (Fig. 6*A*) (20). This reaction is, however, extremely slow. FimA WT monomers assemble to rods at 37 °C with a $t_{½}$ of about 10 days at initial FimA monomer concentrations of 50 μM (Fig. 6, *B* and *C*). The likely reason for this slow assembly reaction is the fact that folded FimA monomers are assembly-incompetent and thus first have to unfold before they can interact with the Nte of another FimA molecule (Fig. 6*A*). Accordingly, the first intermediate in spontaneous FimA polymerization must be a heterodimer (NU) between a folded and an unfolded FimA molecule, because the FimA core (residues 20–159) cannot fold to an intact tertiary structure (14). The following assembly steps would involve the refolding of monomers on the growing oligomers. The subunit incorporation steps are known to be irreversible under

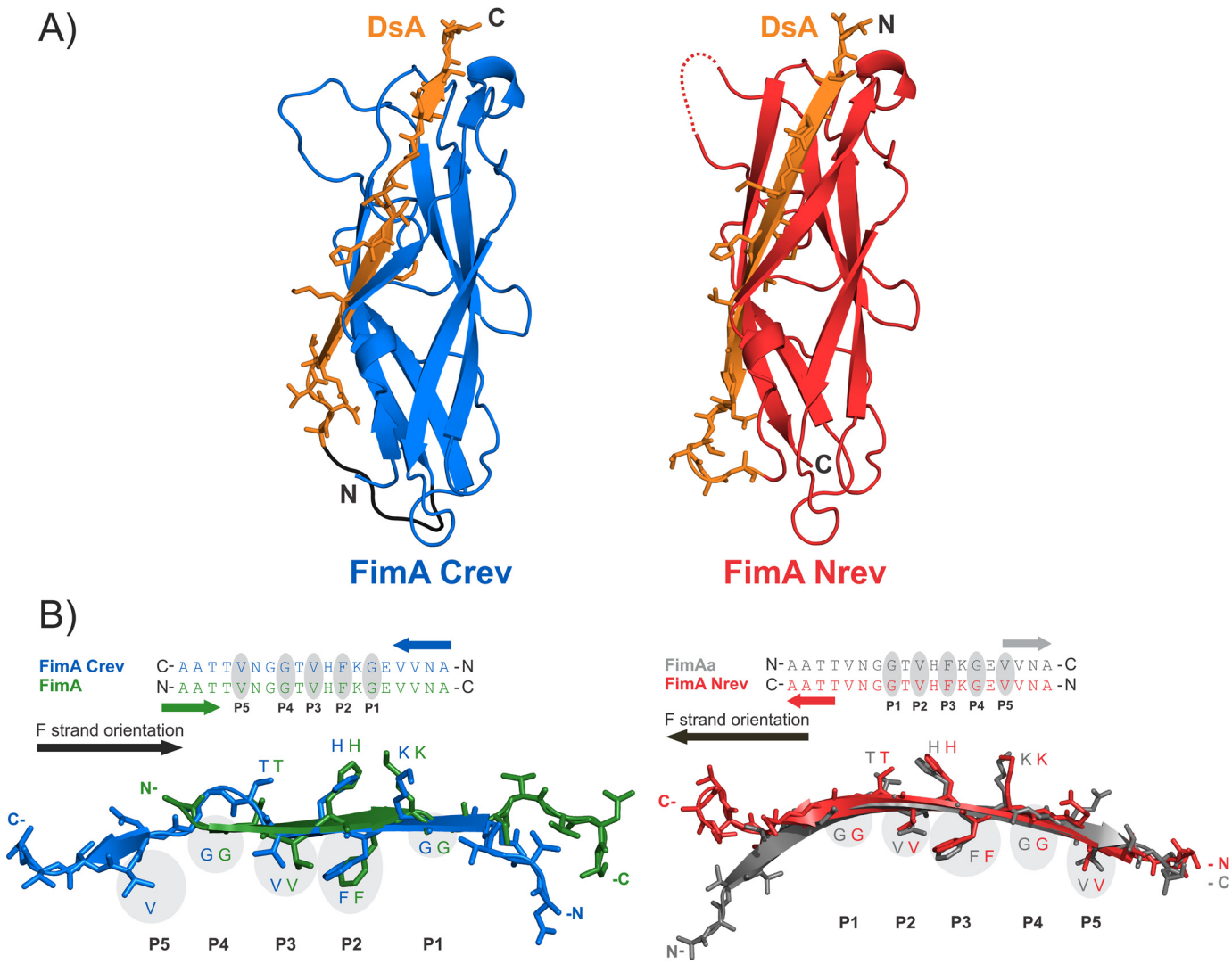

Figure 5. Solved X-ray structures of FimA Nrev and FimA Crev. *A, left*, structure of FimA Crev, with the FimA core (residues 20–159) shown in *blue*, the donor strand in *orange*, and the Gly_6 linker in *black*. *Right*, structure of FimA Nrev, with the protein core shown in *red* and the donor strand in *orange*. Small differences between the solved structures of FimA Nrev and FimA Crev can be observed in the loop segment 90–95 (Fig. S4). The *dashed line* indicates the missing electron density for residues 92 and 93 in the structure of FimA Nrev. *B*, *left*, superposition of the reversely oriented donor strand segments of FimA Crev (*blue*, PDB entry 6S09) and the FimA WT monomer (*green*, PDB entry 5NKT) after global structural alignment of both structures. *Right*, superposition of the reversely oriented donor strand segments of FimA Nrev (*red*, PDB entry 6R74) and FimAa (*gray*, PDB entry 2JTY, NMR model 18) after global structural alignment of both structures. *Gray areas* indicate the binding pockets P1–P5.

physiological conditions (10, 14). The marginal thermodynamic stability of FimA (–5.5 kJ/mol) should favor spontaneous FimA assembly because a significant fraction of the monomers is fully unfolded under physiological conditions. In turn, this implies that stabilization of the native state of the FimA monomer impairs or prevents spontaneous assembly.

To test this hypothesis, we analyzed the ability of homopolymer formation of the strongly stabilized variant FimA Nrev, which has a free energy of folding of –31.5 kJ/mol and an extrapolated $t_{½}$ of the spontaneous unfolding of 60 years (Tables 1 and 2). Indeed, FimA Nrev stayed completely monomeric after incubation for 7 days under conditions where about one-third of WT FimA already had assembled to rods (Fig. 6, *B* and *C*). Besides its stability against unfolding, another reason for the inability of FimA Nrev to form homopolymers could be the lower stability of FimA Nrev homopolymers. As polymerization requires intermolecular, antiparallel donor strand insertion (Figs. 1*B* and 6*A*), homopolymers of FimA Nrev may not be significantly more stable than the monomeric analog FimA Crev (–6.9 kJ/mol; Tables 1 and 2). Consequently, in contrast to WT FimA (Fig. 6*A*) (11), the formation of subunit-subunit contacts may not be irreversible in the case of FimA Nrev and impede the formation of stable pilus rods *in vitro*.

Discussion

The bacterial type 1 pilus subunit FimA differs from most other proteins due to its remarkable ability to fold into two alternative conformations with distinct biological functions. The majority of the FimA molecules assemble to the highly stable helical quaternary structure of the pilus rod, in which the neighboring FimA subunits interact via intermolecular,

Table 3
X-ray data collection and refinement statistics for the crystal structures of FimA Nrev and FimA Crev

	FimA Nrev	FimA Crev
PDB code	6R74	6S09
Wavelength (Å)	1	1
Resolution range (Å)	36.54–1.81 (1.875–1.81)[a]	47.69–1.502 (1.556–1.502)
Space group	R 3 2 :H	P 21 21 21
Unit cell dimensions (Å)	86.55, 86.55, 164.21	92.31, 105.23, 106.99
Unit cell angles (degrees)	90, 90, 120	90, 90, 90
Total reflections	210,185 (10,761)	2,756,133 (126,780)
Unique reflections	21,874 (2146)	165,865 (16,407)
Multiplicity	9.6 (5.0)	16.6 (7.7)
Completeness (%)	99.74 (99.54)	99.96 (99.74)
Mean $I/\sigma(I)$	10.00 (0.90)	5.87 (0.90)
Wilson B-factor (Å^2)	30.27	14.85
R_{meas}	0.1757 (2.018)	0.3763 (2.293)
CC1/2	0.997 (0.578)	0.99 (0.306)
CC*	0.999 (0.856)	0.997 (0.684)
Reflections used in refinement	21,850 (2141)	165,836 (16,384)
Reflections used for R_{free}	1091 (107)	3318 (328)
R_{work}	0.1925 (0.3454)	0.1698 (0.3057)
R_{free}	0.2178 (0.3664)	0.2060 (0.3379)
CC(work)	0.956 (0.749)	0.970 (0.633)
CC(free)	0.892 (0.717)	0.960 (0.578)
No. of nonhydrogen atoms	1221	10,985
Macromolecules	1102	9006
Ligands	30	
Solvent	89	1979
Protein residues	157	1294
RMSD (bonds)	0.003	0.009
RMSD (angles)	0.58	1.02
Ramachandran favored (%)	98.04	97.39
Ramachandran allowed (%)	1.96	2.61
Ramachandran outliers (%)	0.00	0.00
Rotamer outliers (%)	0.00	1.00
Clashscore	2.28	3.28
Average B-factor	44.30	19.96
Macromolecules	43.51	17.66
Ligands	71.65	
Solvent	44.85	30.46
No. of TLS groups	9	58

[a] Values in parentheses indicate the statistics for the highest-resolution shell.

antiparallel donor strand complementation (20, 21). However, a small fraction of the FimA molecules folds to marginally stable, self-complemented monomers that delay apoptosis of urinary epithelial cells after type 1 pilus-mediated internalization of uropathogenic, Gram-negative pathogens (18). The prerequisite for these alternative folding possibilities is the pseudo-palindromic sequence of the β-strand formed by the N-terminal extension of FimA (10, 14, 17). In the present study, we addressed the role of this pseudo-palindromic sequence, which can complete the immunoglobulin-like tertiary structure of FimA by inserting into the FimA fold as a β-strand in opposite orientations, for folding and stability of FimA. We provide convincing evidence that the dramatic difference in thermodynamic stability between the two FimA conformers is determined by the identity of the residues inserting into the donor strand side-chain binding pockets and not, as suggested previously (14, 17), by the orientation or the length of the inserted donor strand. Notably, the FimA fold tolerated the reversed, nonnatural donor strand sequences in our FimA constructs FimA Nrev and FimA Crev. In addition, both FimA variants completely reproduced the characteristic properties of the corresponding natural conformers FimAa and the FimA monomer, respectively, which accommodate identical donor strand side chains in the P1–P5 pockets. These properties are (i) marginal thermodynamic stability and reversible two-state folding in the case of the FimA/FimA Crev pair and (ii) extraordinary stability coupled with kinetically unattained two-state folding in the case of the FimAa/FimA Nrev pair. The residues in the pockets P1, P4, and P5 are identical in all FimA conformers (Gly, Gly, and Val, respectively; see Figs. 1 and 5 and Fig. S3). Thus, the occupancy of the donor strand side chain pockets P2 and P3, which can either accommodate a valine or a phenylalanine side chain, appears to be the main determinant of FimA folding and stability.

Materials and methods

Gene design and cloning of FimA variants

Plasmids for cytoplasmic expression in *E. coli* under T7 promoter control of FimA WT and FimAa were described previously (10, 14). Analogous T7 expression plasmids for FimA Nrev and FimA Crev were generated from synthetic genes (Geneart Thermo Fisher) with standard molecular cloning techniques.

Protein production and purification

The new FimA variants FimA Nrev and FimA Crev described in this study were produced and purified essentially as described previously for FimA and FimAa (10). Proteins were produced in *E. coli* BL21 (DE3) cells (New England Biolabs) harboring the respective expression plasmid. Cells were grown at 37 °C in 2YT medium (16 g/liter tryptone, 10 g/liter yeast extract, 5 g/liter NaCl) containing ampicillin (100 μg/ml). Protein production was induced at $A_{600\,nm} = 0.6$ by the addition of isopropyl 1-thio-β-D-galactopyranoside (1 mM final concentration). Cells were grown for an additional 6 h and harvested by centrifugation. Cells were resuspended (one one-hundredth of the original culture volume) in 100 mM Tris/HCl, pH 8.0, 2 mM $MgCl_2$, 10 μg/ml DNase I, 1.5 mM phenylmethylsulfonyl fluoride containing an EDTA-free protein inhibitor mixture (Roche) and lysed (Microfluidics cell cracker, five passes at 12,000 p.s.i.). The lysate was mixed with 0.8 volumes of 60 mM EDTA, 1.5 M NaCl, pH 7.0, and 6% (v/v) of Triton X-100. The mixture was stirred at 4 °C for 30 min and centrifuged (30 min, 4 °C, 48,000 × *g*) to precipitate inclusion bodies and remove detergent-solubilized membrane proteins. The inclusion bodies were extensively washed with 100 mM Tris/HCl, pH 8.0, and 20 mM EDTA to remove Triton X-100 and nucleic acids and then solubilized at room temperature in 6 M GdmCl, 50 mM Tris/HCl, pH 8.0, 0.1 mM EDTA, 50 mM DTT (5 ml/1 g of inclusion bodies). Insoluble material was removed by ultracentrifugation (30 min, 100,000 × *g*, 20 °C), and DTT and EDTA were removed by buffer exchange on a Sephadex G25 desalting column equilibrated with 6 M GdmCl, 20 mM acetic acid–NaOH, pH 4.0. The reduced, denatured protein was then diluted to ~5 μM with 6 M GdmCl, 50 mM Tris/HCl, pH 8.0, and 0.1 mM $CuCl_2$ and incubated overnight at room temperature for Cu^{2+}-catalyzed air oxidation and formation of the single structural disulfide bond in the FimA variants. The solution was concentrated to a final protein concentration of ~50 μM by cross-flow filtration (5-kDa Hydrosart membrane cassettes, Sartorius), and proteins were refolded by dialysis against 20 mM sodium phosphate, pH 7.0, 150 mM NaCl, and 1 mM EDTA (6–8 kDa

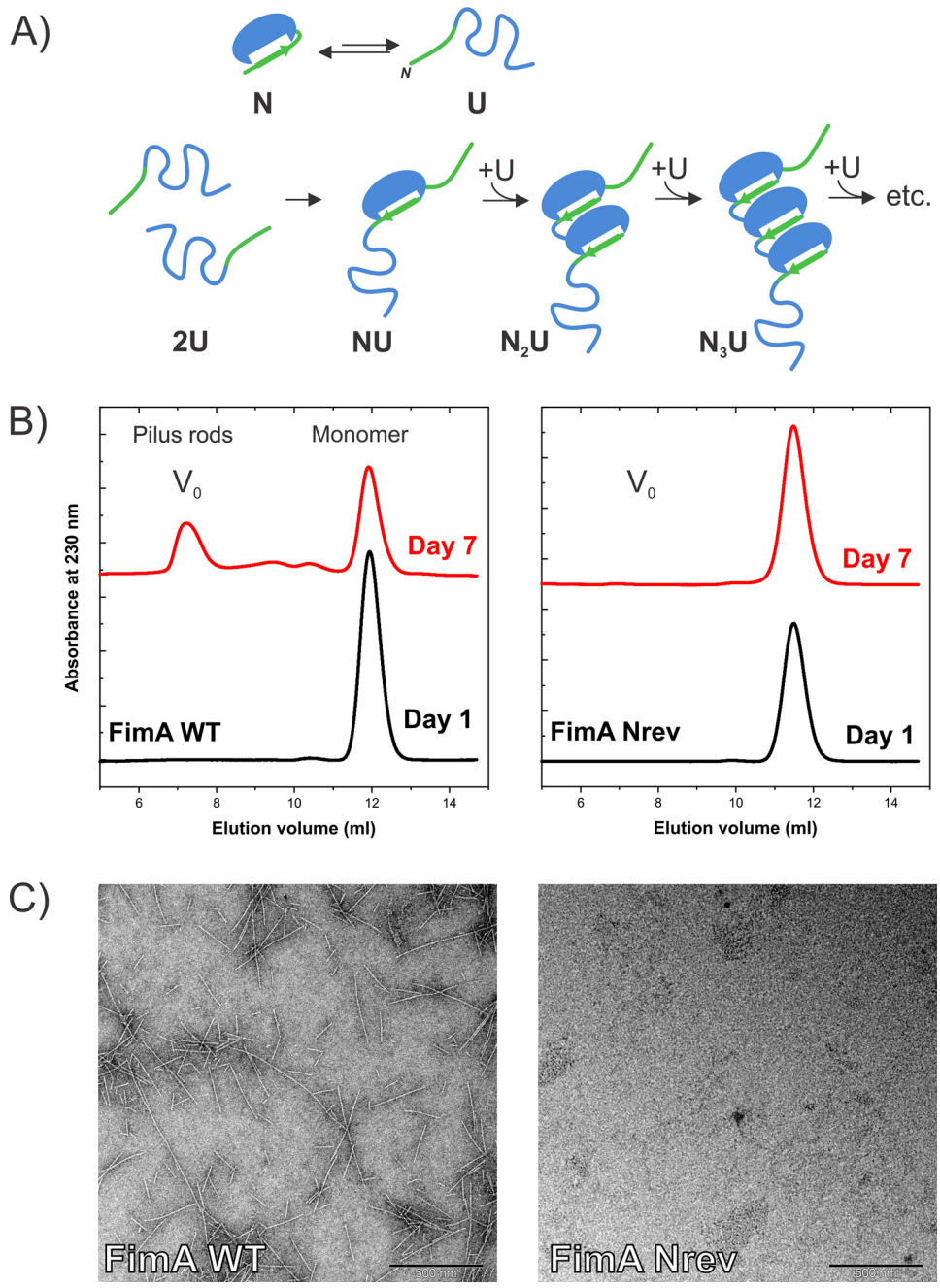

Figure 6. FimA WT monomers spontaneously assemble to pilus rods, whereas the more stable monomers of FimA Nrev remain assembly-incompetent. *A*, model of spontaneous pilus rod assembly from FimA monomers. Folded (*N*) FimA monomers need to unfold (*U*) to become assembly-competent. The first intermediate in this mechanism is an NU heterodimer. Each following step involves the refolding of the incoming monomer on the growing polymer. *B*, gel filtration runs monitoring pilus rod formation from FimA WT and FimA Nrev monomers (50 μM initial concentration). *Left*, the assembly reaction at 37 °C and pH 5.0 was initiated by dissolving lyophilized FimA monomers in assembly buffer and shows a $t_{½}$ of about 10 days in the case of WT FimA. Elution volumes of the monomer and pilus rods (eluting at the void volume V_0) are indicated for samples taken after 1 day and 7 days. *Right*, FimA Nrev stays monomeric under the same conditions. *C*, negative stain EM micrographs of the reactions in *B* after 7 days of incubation, showing that pilus rods were only formed by WT FimA. *Scale bar*, 500 nm.

cut-off membrane, 4 °C, overnight). The refolded proteins were then transferred to 50 mM ammonium bicarbonate by dialysis (3 h, 4 °C) and applied to a Superdex 75 26/60 gel filtration column equilibrated with the same buffer. Fractions containing the pure, native monomers were collected and combined. Portions corresponding to 1 mg of protein were flash-frozen in liquid nitrogen, lyophilized, and stored at −80 °C until further use. Protein masses were verified by electrospray ionization MS (FimA Nrev: calculated: 15,825.36, measured: 15,825.00; FimA Crev: calculated: 16,238.75, measured: 16,238.5). MS confirmed that the N-terminal methionines had been cleaved off. The final yield of purified, native protein was about 35 mg/liter of bacterial culture for each FimA variant.

Protein concentration determination

Concentrations of purified FimA variants were measured via their specific absorbance at 280 nm. As the N-terminal extension of FimA lacks tyrosine and tryptophan residues, all

variants had the same molar extinction coefficient at 280 nm ($\epsilon_{280\ nm}$) of 2680 $M^{-1}\ cm^{-1}$.

Refolding kinetics

Lyophilized proteins were dissolved in 5 mM MOPS/NaOH, pH 7.0, 3.0 M GdmCl to a concentration of 600 μM and incubated for 5 min at 95 °C to ensure complete unfolding. Refolding was initiated by rapid dilution to 10 μM protein concentration with 5 mM MOPS/NaOH, pH 7.0 (final GdmCl concentration: 50 mM). Refolding at 25 °C was monitored by the increase in the far-UV CD signal at 230 nm using a JASCO J-715 spectropolarimeter. The final GdmCl concentration in the refolding reactions was 50 mM and verified via the refractive index (22). Refolding traces were consistent with monoexponential kinetics and fitted with OriginPro 2017 according to Equation 1,

$$S = S_0 + (S_\infty - S_0) \cdot e^{-k_1 t} \qquad \text{(Eq. 1)}$$

where S is the measured CD signal, S_0 is the signal at $t = 0$, S_∞ is the signal at the end of the reaction, k_1 is the rate constant of refolding at 50 mM GdmCl, and t is the refolding time.

Temperature-induced unfolding transitions

Lyophilized proteins were dissolved in 5 mM MOPS/NaOH, pH 7.0, to 10 μM. The far-UV CD signal of the proteins at 230 nm was monitored during heating from 25 to 105 °C at the heating rate of 1 °C/min. Unfolding traces were fitted with OriginPro 2017 according to a two-state van't Hoff transition (Equation 2) (23),

$$S = ((S_f + m_f \cdot T) + (S_u + m_u \cdot T) \cdot \exp(\Delta H_m/(R \cdot T) \cdot (T - T_m)/T_m))/(1 + \exp(\Delta H_m/(R \cdot T) \cdot (T - T_m)/T_m)) \qquad \text{(Eq. 2)}$$

where S is the measured CD signal, S_u and S_f are the signals of unfolded and folded protein at zero K, m_u and m_f are the temperature dependences ("slopes") of the signal of unfolded and native protein, respectively, T_m is the melting temperature, ΔH is the enthalpy of unfolding, R is the gas constant, and T is the temperature in K. The fitted CD trace was then normalized, and the fraction of native molecules was plotted against temperature. We only used the obtained, apparent T_m values as a qualitative measure of thermal stability, because we could not establish complete reversibility of thermal unfolding.

GdmCl-dependent unfolding and refolding transitions with attained or unattained folding equilibrium

Stock solutions of folded (150 μM in 5 mM MOPS/NaOH, pH 7.0) or unfolded proteins (650 μM in 5 mM MOPS/NaOH, pH 7.0, and 3 M GdmCl and incubated for 5 min at 95 °C) were diluted to 15 μM in 5 mM MOPS/NaOH, pH 7.0, buffer containing different GdmCl concentrations and incubated at 25 °C. The far-UV CD signal at 230 nm of each sample was recorded after different incubation times for 30 s and averaged. The final GdmCl concentrations were verified via their refractive indices (22). The recorded CD signals were plotted against GdmCl concentration.

FimA Crev reached folding equilibrium (coinciding unfolding and refolding traces) after 1 day of incubation. The data were fitted according to the two-state model of folding according to Equation 3,

$$S = (m_f \cdot x + s_f) + ((m_u \cdot x + s_u - m_f \cdot x - s_f)/(\exp - (\Delta G^0 + m_{eq} \cdot x)/(R \cdot T)) + 1)) \qquad \text{(Eq. 3)}$$

where S is the measured CD signal, S_u and S_f are the signals of unfolded and native protein at zero denaturant, m_u and m_f are the GdmCl dependences ("slopes") of the signals of unfolded and native protein, respectively, ΔG^0 is the free energy of folding at zero GdmCl, and m_{eq} is the denaturant dependence of ΔG (cooperativity of folding).

The folding equilibrium of FimA Nrev could not be attained at 25 °C and was analyzed according to the theory of an unattained two-state equilibrium using a combination of Equations 4–6, as described previously (24),

$$k_F = k_F^{H_2O} \cdot e^{m_F D} \qquad \text{(Eq. 4)}$$

$$k_U = k_U^{H_2O} \cdot e^{m_U D} \qquad \text{(Eq. 5)}$$

$$f_N(t) = \frac{k_F}{k_F + k_U} + \left(f_N(0) - \frac{k_F}{k_F + k_U}\right) \cdot e^{-(k_F + k_U)t} \qquad \text{(Eq. 6)}$$

where $k_F^{H_2O}$ and k_U^{H2O} are the rate constants of folding and unfolding at zero GdmCl, m_F and m_U are the linear dependences of $\ln(k_U)$ and $\ln(k_F)$ on GdmCl concentration (kinetic m-values), D is the GdmCl concentration, and $f_N(t)$ is the fraction of native molecules after incubation time t. The parameter $f_N(0)$ is zero for unfolding and one for refolding experiments. Equation 6 describes the kinetics of attainment of a two-state folding equilibrium, and Equations 4 and 5 describe the dependence of k_F and k_U on denaturant concentration, respectively. For normalization of the recorded CD signals, Equation 7 was used,

$$f_N = \frac{S - (S_U^0 + m_U D)}{(S_N^0 + m_N D) - (S_U^0 + m_U D)} \qquad \text{(Eq. 7)}$$

where S is the measured CD signal, and S_N^0 and S_U^0 are the signals of the folded and unfolded protein at zero GdmCl, respectively, and m_N and m_U are the GdmCl dependences of S_N and S_U, respectively. As no pretransition baseline for native molecules could be recorded, the m_N was fixed to zero.

The V-plot for the FimA Nrev folding kinetics (Fig. 3*C*) was deduced from the data points in the transition regions between 5 and 95% of folded molecules in Fig. 3*B*. From the fractions of folded molecules and the respective incubation times, the logarithm of the observed rate constants of folding/unfolding ln (k_{obs}) was calculated, plotted against D, and fitted according to Equation 8, with $k_{obs} = k_F + k_U$.

$$\ln k_{obs} = \ln(k_F^{H_2O} \cdot e^{m_F \cdot [D]} + k_U^{H_2O} \cdot e^{m_U \cdot [D]}) \qquad \text{(Eq. 8)}$$

The predicted equilibrium transitions of the FimA Nrev (*dotted lines* in Fig. 3*B*) were calculated from Equation 9,

$$f_N = \frac{e^{-\frac{\Delta G^0_{H_2O} + m_{eq} \cdot D}{RT}}}{e^{-\frac{\Delta G^0_{H_2O} + m_{eq} \cdot D}{RT}} + 1} \quad \text{(Eq. 9)}$$

where $G^0_{H_2O}$ is the free energy of folding at zero denaturant and m_{eq} is the cooperativity of folding (in J mol^{-1} M^{-1}), which equals $(m_U - m_F)\cdot$RT. All data were fitted and plotted in OriginPro 2017.

Crystallization of FimA Nrev and FimA Crev

Commercially available crystallization screens from Hampton Research were used to set up initial sitting-vapor diffusion experiments. Stock solution of FimA Nrev (18 mg/ml) or FimA Crev (20 mg/ml) in 5 mM MOPS/NaOH, pH 7.0, were mixed 1:1 with precipitant solution (96-well plates; 3 Drop IntelliPlate 96-3 LVR) using a Phoenix crystallization robot (Art Robbins Instruments). Screens were set up at room temperature and 4 °C. Crystals of FimA Nrev grew within 120 days at 4 °C in 45% ammonium sulfate, 0.1 M sodium malonate, pH 3.1. Crystals were flash-frozen with liquid nitrogen after the addition of 12% glycerol as cryoprotectant.

Crystals of FimA Crev grew within 5 days at 4 °C in 28% PEG 8000, 0.1 M sodium acetate, pH 4.5, 0.2 M lithium sulfate. A drop of 50% PEG 4000 was used as cryoprotectant, and crystals were flash-frozen in liquid nitrogen.

X-ray data collection and structure determination of FimA Nrev and FimA Crev

Data for FimA Nrev and FimA Crev was collected at X10SA beamline (PXIII) at the Swiss Light Source (PSI, Viligen, Switzerland) with a wavelength of 1 Å and a PILATUS 6M detector. X-ray diffraction data were analyzed with XDS (25) and cut at 1.68 Å for FimA Nrev and 1.50 Å in FimA Crev. Phases were determined by molecular replacement using FimA WT crystal structure (accession number 5NKT) for FimA Nrev and FimA Crev in Phaser from the Phenix software package (26). Model building and refinement were performed in COOT (27) and Phenix. The final R_{free}/R_{work} are 0.1925/0.2178 for FimA Nrev and 0.1698/0.2060 for FimA Crev (see Table 3, Table S1, Table S2, and Fig. S2 for statistics on data collection and refinement).

Structure analysis

Structure alignments were performed pairwise on only C^α atoms in PyMOL 2.1 using the *align* command. Aligned structures were further analyzed using a Python script to calculate the RMSD between two C^α atoms occupying the same positions in the hydrophobic groove of FimA core. Obtained values were plotted against the position in the strand. Interactions between donor strands and the FimA core were analyzed with the COCOMAPS web server (28). For this purpose, donor strand segments were defined as separate chains, and default server settings were used (8-Å cutoff).

Spontaneous assembly of FimA variants into pilus rods

Lyophilized FimA or FimA Nrev was dissolved in 150 mM NaCl, 20 mM acetic acid/NaOH, pH 5.0, to a protein concentration of 50 μM and incubated at 37 °C. Samples were analyzed by analytical gel filtration on a Superdex 75 10/300 column equilibrated with 150 mM NaCl, 50 mM Tris/HCl, pH 8.0, immediately after the onset of the assembly reactions or after 1 week. The rest of the samples were incubated at 37 °C for 1 week. For the preparation of negative stain EM grids, aliquots (3 µl) were removed from the respective reaction mixture and stained with 2% phosphotungstic acid at pH 7.2. Micrographs were recorded on FEI Morgagni 268 at 8000-fold magnification.

Data availability

Structures presented in this paper have been deposited to the Protein Data Bank with the following accession codes: 6R74, 6S09, and 6R7E.

Acknowledgments—We thank the Functional Genomics Center Zurich, especially Dr. S. Chesnov, for help with measuring the mass spectra of proteins; the Protein Crystallization center and B. Blattmann for help with setting up the crystallization screens; and Dr. V. Olieric from the Swiss Light Source for assistance with X-ray data acquisition. We thank Dr. M. Hospenthal, Dr. S. Przetocka, and P. Bachmann for helpful comments.

Author contributions—D. Z. and R. G. conceptualization; D. Z. and B. E. data curation; D. Z. software; D. Z. and B. E. formal analysis; D. Z. and R. G. supervision; D. Z., B. E., and R. G. validation; D. Z., B. E., and R. G. investigation; D. Z. and B. E. visualization; D. Z., B. E., and R. G. methodology; D. Z., B. E., and R. G. writing-original draft; D. Z. and R. G. project administration; D. Z., B. E., and R. G. writing-review and editing; R. G. resources; R. G. funding acquisition.

Funding and additional information—This work was supported by Swiss National Science Foundation Grants 310030B_176403/1 and 31003A_156304 (to R. G.).

Conflict of interest—The authors declare that they have no conflicts of interest with the contents of this article.

Abbreviations—The abbreviations used are: UPEC, uropathogenic *Escherichia coli*; Nte, N-terminal extension; Cte, C-terminal extension; GdmCl, guanidinium chloride; PDB, Protein Data Bank; RMSD, root mean square deviation.

References

1. Ronald, A. (2003) The etiology of urinary tract infection: traditional and emerging pathogens. *Dis. Mon.* **49,** 71–82 CrossRef Medline
2. Sauer, M. M., Jakob, R. P., Luber, T., Canonica, F., Navarra, G., Ernst, B., Unverzagt, C., Maier, T., and Glockshuber, R. (2019) Binding of the bacterial adhesin FimH to its natural, multivalent high-mannose type glycan targets. *J. Am. Chem. Soc.* **141,** 936–944 CrossRef Medline
3. Hospenthal, M. K., and Waksman, G. (2019) The remarkable biomechanical properties of the type 1 chaperone-usher pilus: a structural and molecular perspective. *Microbiol. Spectr.* **7,** CrossRef Medline
4. Flores-Mireles, A. L., Walker, J. N., Caparon, M., and Hultgren, S. J. (2015) Urinary tract infections: epidemiology, mechanisms of infection and treatment options. *Nat. Rev. Microbiol.* **13,** 269–284 CrossRef Medline

5. Thanassi, D. G., Saulino, E. T., and Hultgren, S. J. (1998) The chaperone/usher pathway: a major terminal branch of the general secretory pathway. *Curr. Opin. Microbiol.* **1,** 223–231 CrossRef Medline
6. Crespo, M. D., Puorger, C., Schärer, M. A., Eidam, O., Grütter, M. G., Capitani, G., and Glockshuber, R. (2012) Quality control of disulfide bond formation in pilus subunits by the chaperone FimC. *Nat. Chem. Biol.* **8,** 707–713 CrossRef Medline
7. Vetsch, M., Erilov, D., Molière, N., Nishiyama, M., Ignatov, O., and Glockshuber, R. (2006) Mechanism of fibre assembly through the chaperone-usher pathway. *EMBO Rep.* **7,** 734–738 CrossRef Medline
8. Geibel, S., Procko, E., Hultgren, S. J., Baker, D., and Waksman, G. (2013) Structural and energetic basis of folded-protein transport by the FimD usher. *Nature* **496,** 243–246 CrossRef Medline
9. Nishiyama, M., Horst, R., Eidam, O., Herrmann, T., Ignatov, O., Vetsch, M., Bettendorff, P., Jelesarov, I., Grütter, M. G., Wüthrich, K., Glockshuber, R., and Capitani, G. (2005) Structural basis of chaperone-subunit complex recognition by the type 1 pilus assembly platform FimD. *EMBO J.* **24,** 2075–2086 CrossRef Medline
10. Żyła, D. S., Prota, A. E., Capitani, G., and Glockshuber, R. (2019) Alternative folding to a monomer or homopolymer is a common feature of the type 1 pilus subunit FimA from enteroinvasive bacteria. *J. Biol. Chem.* **294,** 10553–10563 CrossRef Medline
11. Puorger, C., Eidam, O., Capitani, G., Erilov, D., Grütter, M. G., and Glockshuber, R. (2008) Infinite kinetic stability against dissociation of supramolecular protein complexes through donor strand complementation. *Structure* **16,** 631–642 CrossRef Medline
12. Barnhart, M. M., Pinkner, J. S., Soto, G. E., Sauer, F. G., Langermann, S., Waksman, G., Frieden, C., and Hultgren, S. J. (2000) PapD-like chaperones provide the missing information for folding of pilin proteins. *Natl. Acad. Sci. U. S. A.* **97,** 7709–7714 CrossRef Medline
13. Barnhart, M. M., Sauer, F. G., Pinkner, J. S., and Hultgren, S. J. (2003) Chaperone-subunit-usher interactions required for donor strand exchange during bacterial pilus assembly. *J. Bacteriol.* **185,** 2723–2730 CrossRef Medline
14. Puorger, C., Vetsch, M., Wider, G., and Glockshuber, R. (2011) Structure, folding and stability of FimA, the main structural subunit of type 1 pili from uropathogenic *Escherichia coli* strains. *J. Mol. Biol.* **412,** 520–535 CrossRef Medline
15. Alonso-Caballero, A., Schönfelder, J., Poly, S., Corsetti, F., De Sancho, D., Artacho, E., and Perez-Jimenez, R. (2018) Mechanical architecture and folding of *E. coli* type 1 pilus domains. *Nat. Commun.* **9,** 2758 CrossRef Medline
16. Hahn, E., Wild, P., Hermanns, U., Sebbel, P., Glockshuber, R., Häner, M., Taschner, N., Burkhard, P., Aebi, U., and Müller, S. A. (2002) Exploring the 3D molecular architecture of *Escherichia coli* type 1 pili. *J. Mol. Biol.* **323,** 845–857 CrossRef Medline
17. Walczak, M. J., Puorger, C., Glockshuber, R., and Wider, G. (2014) Intramolecular donor strand complementation in the *E. coli* type 1 pilus subunit FimA explains the existence of FimA monomers as off-pathway products of pilus assembly that inhibit host cell apoptosis. *J. Mol. Biol.* **426,** 542–549 CrossRef Medline
18. Sukumaran, S. K., Fu, N. Y., Tin, C. B., Wan, K. F., Lee, S. S., and Yu, V. C. (2010) A soluble form of the pilus protein FimA targets the VDAC-hexokinase complex at mitochondria to suppress host cell apoptosis. *Mol. Cell* **37,** 768–783 CrossRef Medline
19. Nishiyama, M., Ishikawa, T., Rechsteiner, H., and Glockshuber, R. (2008) Reconstitution of pilus assembly reveals a bacterial outer membrane catalyst. *Science* **320,** 376–379 CrossRef Medline
20. Hospenthal, M. K., Zyla, D., Costa, T. R. D., Redzej, A., Giese, C., Lillington, J., Glockshuber, R., and Waksman, G. (2017) The cryoelectron microscopy structure of the type 1 chaperone-usher pilus rod. *Structure* **25,** 1829–1838.e4 CrossRef Medline
21. Spaulding, C. N., and Hultgren, S. J. (2016) Adhesive pili in UTI pathogenesis and drug development. *Pathogens* **5,** 30 CrossRef Medline
22. Nozaki, Y. (1972) The preparation of guanidine hydrochloride. *Methods Enzymol.* **26,** 43–50 CrossRef Medline
23. Mergny, J.-L., and Lacroix, L. (2003) Analysis of thermal melting curves. *Oligonucleotides* **13,** 515–537 CrossRef Medline
24. Erilov, D., Puorger, C., and Glockshuber, R. (2007) Quantitative analysis of nonequilibrium, denaturant-dependent protein folding transitions. *J. Am. Chem. Soc.* **129,** 8938–8939 CrossRef Medline
25. Kabsch, W. (2010) XDS. *Acta Crystallogr. D Biol. Crystallogr.* **66,** 125–132 CrossRef Medline
26. Adams, P. D., Afonine, P. V., Bunkóczi, G., Chen, V. B., Davis, I. W., Echols, N., Headd, J. J., Hung, L.-W., Kapral, G. J., Grosse-Kunstleve, R. W., McCoy, A. J., Moriarty, N. W., Oeffner, R., Read, R. J., Richardson, D. C., *et al.* (2010) PHENIX: a comprehensive Python-based system for macromolecular structure solution. *Acta Crystallogr. D Biol. Crystallogr.* **66,** 213–221 CrossRef Medline
27. Emsley, P., Lohkamp, B., Scott, W. G., and Cowtan, K. (2010) Features and development of Coot. *Acta Crystallogr. D Biol. Crystallogr.* **66,** 486–501 CrossRef Medline
28. Vangone, A., Spinelli, R., Scarano, V., Cavallo, L., and Oliva, R. (2011) COCOMAPS: a web application to analyze and visualize contacts at the interface of biomolecular complexes. *Bioinformatics* **27,** 2915–2916 CrossRef Medline
29. Eisenberg, D., Schwarz, E., Komaromy, M., and Wall, R. (1984) Analysis of membrane and surface protein sequences with the hydrophobic moment plot. *J. Mol. Biol.* **179,** 125–142 CrossRef Medline